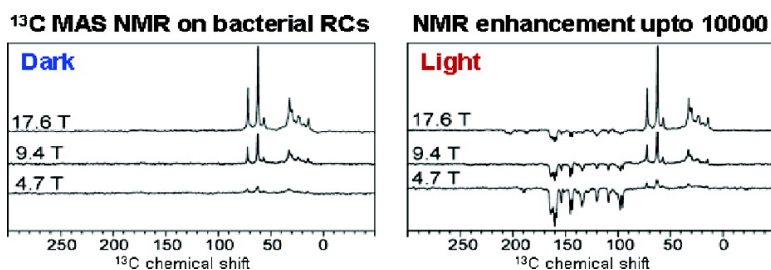Article

Magnetic Field Dependence of Photo-CIDNP MAS NMR on Photosynthetic Reaction Centers of *Rhodobacter sphaeroides* WT

Shipra Prakash, Alia, Peter Gast, Huub J. M. de Groot, Gunnar Jeschke, and Jrg Matysik

More About This Article

Additional resources and features associated with this article are available within the HTML version:

- Supporting Information
- Links to the 3 articles that cite this article, as of the time of this article download
- Access to high resolution figures
- Links to articles and content related to this article
- Copyright permission to reproduce figures and/or text from this article

View the Full Text HTML

Magnetic Field Dependence of Photo-CIDNP MAS NMR on Photosynthetic Reaction Centers of *Rhodobacter sphaeroides* WT

Shipra Prakash,[†] Alia,[†] Peter Gast,[‡] Huub J. M. de Groot,[†] Gunnar Jeschke,[§] and Jörg Matysik*,[†]

Contribution from the Leiden Institute of Chemistry, Leiden University, P.O. Box 9502, 2300 RA Leiden, The Netherlands, Department of Biophysics, Leiden University, P.O. Box 9504, 2300 RA Leiden, The Netherlands, and Max-Planck-Institute für Polymerforschung, Postfach 3148, 55021 Mainz, Germany

Received June 17, 2005; E-mail: j.matysik@chem.leidenuniv.nl

Abstract: Photochemically induced dynamic nuclear polarization (photo-CIDNP) is observed in frozen and quinone depleted photosynthetic reaction centers of the purple bacteria *Rhodobacter sphaeroides* wild type (WT) by ^{13}C solid-state NMR at three different magnetic fields. All light-induced signals appear to be emissive at all three fields. At 4.7 T (200 MHz proton frequency), the strongest enhancement of NMR signals is observed, which is more than 10 000 above the Boltzmann polarization. At higher fields, the enhancement factor decreases. At 17.6 T, the enhancement factor is about 60. The field dependence of the enhancement appears to be the same for all nuclei. The observed field dependence is in line with simulations that assume two competing mechanisms of polarization transfer from electrons to nuclei, three-spin mixing (TSM) and differential decay (DD). These simulations indicate a ratio of the electron spin density on the special pair cofactors is 3:2 in favor of the L-BChl during the radical cation state. The good agreement of simulations with the experiments raises expectations that artificial solid reaction centers can be tuned to show photo-CIDNP in the near future.

Introduction

Solid state NMR is a rapidly developing technique for the study of samples, such as membrane proteins, that are difficult to tackle by solution NMR or diffraction methods. Magic-angle spinning (MAS) overcomes line broadening by chemical shift anisotropy (CSA) in solids and allows detailed analysis of structure, dynamics, and functional mechanisms of membrane-bound protein systems.[1,2] The central drawback of NMR methods is their low sensitivity due to an unfavorable Boltzmann distribution caused by the small Zeeman splitting of nuclear spin levels. This general problem of sensitivity in NMR is even more evident in the case of solids, due to lower resolution in terms of achievable line widths relative to the chemical shift range. To improve sensitivity of solid-state NMR several strategies have been developed. Usage of ultrahigh fields increases Zeeman splitting and chemical shift dispersion and can allow, especially in conjunction with pattern labeling and multidimensional data analysis, full backbone and side-chain assignment of proteins.[3-5] Cross-polarization (CP) allows

transfer of magnetization from highly polarized nuclei to those having lower polarization.[6,7] The theoretical enhancement factor is given by the ratio of the gyromagnetic constants. In a typical case, ^{1}H→^{13}C CP, using the proton bath to enhance ^{13}C signals, the enhancement is by a factor of 4. Recently, there has been tremendous progress in the use of dynamic nuclear polarization (DNP) for MAS NMR.[8,9] In these experiments, stable radicals are incorporated into the sample, and the thermal equilibrium polarization of the electron spins is transferred to nuclei under microwave irradiation by a thermal mixing mechanism. Because of the much larger magnetic moment of electron spins compared to nuclear spins, theoretical enhancements are as large as 660 and 2600 for ^{1}H and ^{13}C, respectively. Another strategy to enhance NMR intensities in solids relies on optical pumping by *polarized* electromagnetic radiation.[10,11] In inorganic semi-conductors, near-infrared laser excitation of unpolarized valence-band electrons produces spin-polarized electron−hole pairs which polarize nuclear spins to which they are coupled. In atomic systems, such as alkali atoms containing unpaired electrons, pumping optical transitions with circularly polarized

---

[†] Leiden Institute of Chemistry, Leiden University.
[‡] Department of Biophysics, Leiden University.
[§] Max-Planck-Institute für Polymerforschung.

(1) de Groot, H. J. M. *Curr. Opin. Struct. Biol.* **2000**, *10*, 593−600.
(2) Laws, D. D.; Bitter, H. M. L.; Jerschow, A. *Angew. Chem., Int. Ed.* **2002**, *41*, 3096−3129.
(3) Pauli, J.; Baldus, M.; van Rossum, B.; de Groot, H.; Oschkinat, H. *Chembiochem* **2001**, *2*, 272−281.
(4) Castellani, F.; van Rossum, B.; Diehl, A.; Schubert, M.; Rehbein, K.; Oschkinat, H. *Nature* **2002**, *420*, 98−102.

(5) McDermott, A.; Polenova, T.; Bockmann, A.; Zilm, K. W.; Paulsen, E. K.; Martin, R. W.; Montelione, G. T. *J. Biomol. NMR* **2000**, *16*, 209−219.
(6) Hartmann, S. R.; Hahn, E. L. *Phys. Rev.* **1962**, *128*, 2042−&.
(7) Pines, A.; Gibby, M. G.; Waugh, J. S. *J. Chem. Phys.* **1973**, *59*, 569−590.
(8) Hall, D. A.; Maus, D. C.; Gerfen, G. J.; Inati, S. J.; Becerra, L. R.; Dahlquist, F. W.; Griffin, R. G. *Science* **1997**, *276*, 930−932.
(9) Hu, K. N.; Yu, H. H.; Swager, T. M.; Griffin, R. G. *J. Am. Chem. Soc.* **2004**, *126*, 10844−10845.
(10) Suter, D.; Mlynek, J. *Adv. Magn. Opt. Reson.* **1991**, *16*, 1−83.
(11) Tycko, R.; Reimer, J. A. *J. Phys. Chem.* **1996**, *100*, 13240−13250.

radiation results in selective excitation within the Zeeman-perturbed energy levels via the selection rules for electric dipole transitions. In "transferred optically pumped NMR" (TOPNMR), this magnetization is transferred to noble gases[12,13] such as ^{129}Xe or to biological relevant nuclei such as ^{31}P.[14]

Photochemically induced dynamic nuclear polarization (photo-CIDNP) is a method to increase NMR intensities by induction of photochemical reactions, which shuffle the nuclear spin system out of its Boltzmann equilibrium. In contrast to optical pumping, photo-CIDNP does not require polarized radiation. Photo-CIDNP in solution NMR[15,16] is explained by the radical-pair mechanism which relies on the different chemical fate of diffusing nuclear-spin selected reaction products.[17,18] This mechanism is not feasible in the solid state or for cyclic reactions.

In the solid state, photo-CIDNP has been observed for the first time in quinone blocked frozen bacterial reaction centers (RCs) of *Rhodobacter* (*Rb.*) *sphaeroides* R26[19−21,22] and WT[23,24] under continuous illumination with white light at 9.4 T, allowing an enhancement factor of about 200 to 1000. Plant reaction centers have been studied under the same conditions, and similar enhancement factors were observed. Studies on photosystem I of spinach lead to an almost complete set of assignments of the aromatic ring carbons to the P2 cofactor of the primary electron donor P700.[25] In the D1D2 complex of the RC of the photosystem II of plants, the observation of the pronounced electron density on rings III and V by photo-CIDNP MAS NMR was taken as an indication for a local electric field, leading to a hypothesis about the origin of the remarkable strength of the redox potential of the primary electron donor P680.[26,27] Combining photo-CIDNP at 9.4 T with selective ^{13}C-isotope labeling, two-dimensional photo-CIDNP MAS NMR spectra were obtained, which demonstrated that the electron density in the two bacteriochlorophyll (BChl) molecules of the special pair (P) of a bacterial RC is already asymmetric in its electronic ground state.[24] Furthermore, NMR signals were detected in entire membrane bound bacterial photosynthetic units (>1.5 MDa) with the same label pattern.[28]

The possibility of observing photo-CIDNP in photosynthetic RCs has been predicted already two decades ago,[29] since both

magnetic field effect[30,31] and photochemically induced dynamic *electron* polarization (photo-CIDEP)[32,33] were interpreted in terms of electron−nuclear interactions, although the exact mechanism had not been understood (for historical review, see ref 34). Upon photochemical excitation of the primary electron donor P, which is in bacterial RCs from *Rb. sphaeroides* a dimer assembled from the two BChl cofactors L and M, an electron is emitted to the primary acceptor, a bacteriopheophytin (BPhe) molecule Φ, forming an electron polarized singlet radical pair (Figure 1). In quinone reduced or depleted RCs, further electron transfer is blocked. Therefore, the singlet radical pair can either relax to the electronic ground state or, depending on the strength of the applied magnetic field, be transferred to a triplet radical pair. The triplet radical pair recombines to a special pair triplet ^{3}P and an acceptor singlet. Finally the special pair triplet also relaxes to the singlet ground state, so that the whole process is cyclic and no net effect on the nuclei due to the branching of the reaction pathway would be expected.

Initially, the net nuclear polarization providing photo-CIDNP in solids was assumed to be due to the significant differential relaxation (DR) between the nuclear spins in the special pair triplet ^{3}P and the nuclear spins in the singlet ground state of P, which would break the symmetry between the two branches.[19] Meanwhile, it has been demonstrated experimentally[20,23,24,35] and theoretically[36] that the DR mechanism does not have much significance for bacterial RCs. Currently, two further mechanisms are under discussion.[36] In the electron−electron−nuclear three-spin mixing (TSM) mechanism, net nuclear polarization is created in the spin-correlated radical pair due to the presence of both anisotropic hyperfine interaction and coupling between the two electron spins.[37] In the Differential Decay (DD) mechanism, a net photo-CIDNP effect is caused by anisotropic hyperfine coupling without an explicit requirement for electron−electron coupling if spin-correlated radical pairs have different lifetimes in their singlet and triplet states.[38] Quantification of the contributions and a better understanding of the interplay between TSM and DD mechanisms, however, require further studies. As the two contributions may have different signs,[36] control over both mechanisms may provide a tool to drive intensities in MAS NMR experiments far beyond the Boltzmann state. The field dependence of photo-CIDNP is of particular relevance for such studies. For studying the field dependence of photo-CIDNP, we have chosen the RC of *Rb. sphaeroides* WT, since its kinetics is well-known and, due to the short triplet lifetime of 100 ns, comparatively simple (for review, see ref 39). The good agreement between the experimental data, obtained at 4.7 T (200 MHz proton frequency), 9.4 T (400 MHz), and 17.6 T (750 MHz), and the theoretical simulations, reported in this paper, suggests that a new method to overcome

(12) Raftery, D.; Chmelka, B. F. *Nucl. Magn. Reson.* **1994**, *30*, 112.
(13) Cherubini, A.; Bifone, A. *Prog. Nucl. Magn. Reson. Spectrosc.* **2003**, *42*, 1−30.
(14) Tycko, R. *Sol. State Nucl. Magn. Reson.* **1998**, *11*, 1−9.
(15) Hore, P. J.; Broadhurst, R. W. *Prog. Nucl. Magn. Reson. Spectrosc.* **1993**, *25*, 345−402.
(16) Goez, M. *Adv. Photochem.* **1997**, *23*, 63−164.
(17) Closs, G. L.; Closs, L. E. *J. Am. Chem. Soc.* **1969**, *91*, 4549−4550.
(18) Kaptein, R.; Oosterhoff, J. L. *Chem. Phys. Lett.* **1969**, *4*, 195−197.
(19) Zysmilich, M. G.; McDermott, A. *J. Am. Chem. Soc.* **1994**, *116*, 8362−8363.
(20) Zysmilich, M. G.; McDermott, A. *J. Am. Chem. Soc.* **1996**, *118*, 5867−5873.
(21) Zysmilich, M. G.; McDermott, A. *Proc. Natl. Acad. Sci. U.S.A.* **1996**, *93*, 6857−6860.
(22) Matysik, J.; Alia; Hollander, J. G.; Egorova-Zachernyuk, T.; Gast, P.; de Groot, H. J. M. *Indian J. Biochem. Biophys.* **2000**, *37*, 418−423.
(23) Matysik, J.; Alia; Gast, P.; Lutgenburg, J.; Hoff, A. J.; de Groot, H. J. M. In *Perspectives on Solid State NMR in Biology*; Kiihne, S.; de Groot, H. J. M., Eds.; Kluwer: Dodrecht, 2001; pp 215−225.
(24) Schulten, E. A. M.; Matysik, J.; Alia; Kiihne, S.; Raap, J.; Lutgenburg, J.; Gast, P.; Hoff, A. J.; de Groot, H. J. M. *Biochemistry* **2002**, *41*, 8708−8717.
(25) Alia; Roy, E.; Gast, P.; van Gorkom, H. J.; de Groot, H. J. M.; Jeschke, G.; Matysik, J. *J. Am. Chem. Soc.* **2004**, *126*, 12819−12826.
(26) Matysik, J.; Alia; Gast, P.; van Gorkom, H. J.; Hoff, A. J.; de Groot, H. J. M. *Proc. Natl. Acad. Sci. U.S.A.* **2000**, *97*, 9865−9870.
(27) Diller, A.; Alia; Roy, E.; Gast, P.; van Gorkom, H. J.; de Groot, H. J. M.; Zaanen, J.; Glaubitz, C.; Matysik, J. *Photosynth. Res.* **2005**, *84*, 303−308.

(28) Prakash, S.; Alia; Gast, P.; Jeschke, G.; de Groot, H. J. M.; Matysik, J. *J. Mol. Struct.* **2003**, *661*, 625−633.
(29) Goldstein, R. A.; Boxer, S. G. *Biophys. J.* **1987**, *51*, 937−946.
(30) Blankenship, R. E.; Schaafsma, T. J.; Parson, W. W. *Biochim. Biophys. Acta* **1977**, *461*, 297−305.
(31) Hoff, A. J.; Rademaker, H.; van Grondelle, R.; Duysens, L. N. M. *Biochim. Biophys. Acta* **1977**, *460*, 547−554.
(32) Blankenship, R. E.; McGuire, A.; Sauer, K. *Proc. Natl. Acad. Sci. U.S.A.* **1975**, *72*, 4943−4947.
(33) Hoff, A. J.; Gast, P.; Romijn, J. C. *FEBS Lett.* **1977**, *73*, 185−190.
(34) Hoff, A. J. *Q. Rev. Biophys.* **1981**, *14*, 599−665.
(35) Matysik, J.; Schulten, E.; Alia; Gast, P.; Raap, J.; Lutgenburg, J.; Hoff, A. J.; de Groot, H. J. M. *Biol. Chem.* **2001**, *382*, 1271−1276.
(36) Jeschke, G.; Matysik, J. *Chem. Phys.* **2003**, *294*, 239−255.
(37) Jeschke, G. *J. Am. Chem. Soc.* **1998**, *120*, 4425−4429.
(38) Polenova, T.; McDermott, A. E. *J. Phys. Chem. B* **1999**, *103*, 535−548.
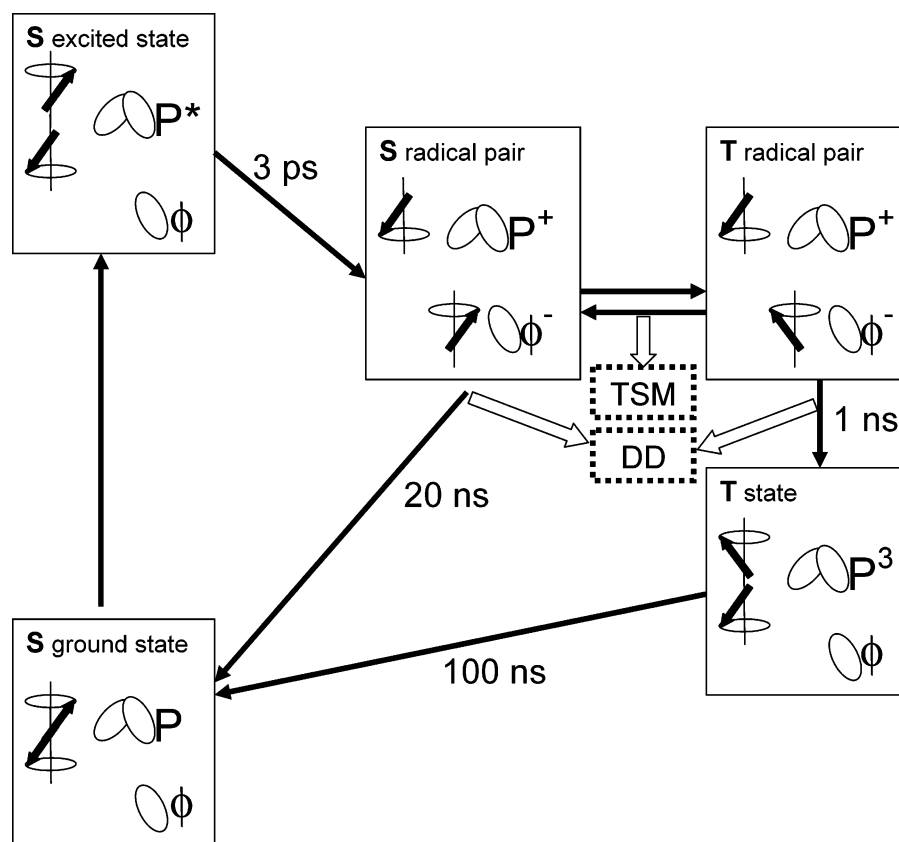(39) Hoff, A. J.; Deisenhofer, J. *Phys. Rep.* **1997**, *287*, 2−247.

Figure 1. Reaction cycle in quinone blocked bacterial RCs. After light-induced electron transfer from the primary donor (P) to the bacteriopheophytin (ϕ), an electron polarized singlet radical pair is formed. The electron polarization is transferred to nuclei via three-spin mixing (TSM) within the radical pair and via differential decay (DD), the difference in lifetime of the two radical pair states.

the intrinsic insensitivity and nonselectivity of MAS NMR can become reality.

Materials and Methods

Sample Preparation. The RCs from *Rb. sphaeroides* WT were isolated as described by Shochat et al.[40] Removal of Q_A was achieved by incubating the RCs at a concentration of 0.6 μM in 4% LDAO, 10 mM *o*-phenanthroline, 10 mM Tris buffer, pH 8.0, for 6 h at 26 °C, followed by washing with 0.5 M NaCl in 10 mM Tris buffer, pH 8.0, containing 0.025% LDAO and 1 mM EDTA.[41] Approximately 15 mg of the RC protein complex embedded in LDAO micelles were used for NMR measurements.

MAS NMR Measurements. The NMR experiments at different fields were performed with AV-750, DMX-400, and DMX-200 NMR spectrometers equipped with magic-angle spinning (MAS) probes. The sample was loaded into a clear 4-mm sapphire rotor and inserted into the MAS probe. It was then frozen slowly at a low spinning frequency of $\nu_r = 400$ Hz to ensure a homogeneous sample distribution against the rotor wall.[42] The light and dark spectra were collected with a Hahn echo pulse sequence and TPPM proton decoupling.[43] ^{13}C MAS NMR spectra were obtained at a temperature of 223 K under continuous illumination with white light.[22]

The rotational frequency for MAS was 8 kHz. For the three fields of 4.7, 9.6, and 17.6 T, a line broadening of 20, 50, and 120 Hz,

(40) Shochat, S.; Arlt, T.; Francke, C.; Gast, P.; Vannoort, P. I.; Otte, S. C. M.; Schelvis, H. P. M.; Schmidt, S.; Vijgenboom, E.; Vrieze, J.; Zinth, W.; Hoff, A. J. *Photosynth. Res.* **1994**, *40*, 55−66.
(41) Okamura, M. Y.; Isaacson, R. A.; Feher, G. *Proc. Natl. Acad. Sci. U.S.A.* **1975**, *72*, 3491−3495.
(42) Fischer, M. R.; de Groot, H. J. M.; Raap, J.; Winkel, C.; Hoff, A. J.; Lugtenburg, J. *Biochemistry* **1992**, *31*, 11038−11049.
(43) Bennett, A. E.; Rienstra, C. M.; Auger, M.; Lakshmi, K. V.; Griffin, R. G. *J. Chem. Phys.* **1995**, *103*, 6951−6958.

respectively, was applied prior to Fourier transformation. At all fields, a cycle delay of 4 s was used. All the ^{13}C-MAS NMR spectra were referenced to the ^{13}COOH response of solid tyrosine·HCl at 172.1 ppm.

The tyrosine spectrum was phased by using zeroth-order phase correction until all signals were absorptive (positive). A small first-order phase correction was applied to correct slight line shape asymmetry of the signals far from the center. The same set of phase correction parameters has been applied to the dark and photo-CIDNP spectra of the RC.

Simulations. Numerical simulations of the photo-CIDNP effect were based on the theory described in ref 36 as implemented in a home-written Matlab program for density matrix computation using the EasySpin library.[44] The program starts from a pure singlet state of the pair and computes time evolution under a Hamiltonian including electron Zeeman, nuclear Zeeman, and hyperfine interaction as well as dipole−dipole and exchange coupling between the two electron spins. The part of the density matrix that decays to the ground state from either singlet or triplet radical pairs is projected out (diamagnetic part) and is further evolved under a Hamiltonian including only the nuclear Zeeman interaction. Evolution is continued until radical pairs have completely decayed (100 ns), and after that, nuclear polarization of the diamagnetic part of the density matrix is determined. As an extension of the approach described in ref 36, this procedure is performed for a full powder average, describing all interactions by tensors, except for the nuclear Zeeman interaction whose anisotropy is negligible on a time scale of 100 ns. A spherical grid (EasySpin function *sphgrid*) with 16 knots and C_i symmetry (481 orientations) was found to be sufficient for powder averaging. Nuclear polarization was normalized to the thermal polarization at the measurement temperature of 223 K.

(44) Stoll, S. Ph.D. Thesis, ETH, Zürich, 2003.

As far as possible, parameters were taken from experimental work. Missing parameters were obtained by density functional theory (DFT) computations (see below). A lifetime of triplet radical pairs of 1 ns, a lifetime of singlet radical pairs of 20 ns, an exchange coupling $J = 7$ G, and a dipole−dipole coupling $d = 5$ G were assumed.[45−47] The principal values of the g tensor of the donor cation radical were taken as 2.003 29, 2.002 39, and 2.002 03.[48] For the g tensor of the acceptor anion radical, we resorted to the values 2.004 37, 2.003 40, and 2.002 39 for the bacteriopheophytin anion radical in *R. viridis*,[49] which we assume to be much closer to actual values for *Rb. sphaeroides* than values computed by DFT. Principal values of ^{13}C hyperfine tensors as well as all tensor principal axis systems were obtained by DFT.

DFT computations were performed with the program ADF 2004.1[50] using the BLYP functional. The starting geometry was taken from the crystal structure of the photosynthetic reaction center of *Rb. sphaeroides* R26[51] in the charge-neutral state (PDB identifier 1AIJ). The two chlorophyll molecules of the special pair as well as the two directly coordinated histidine residues (His L 173 and His M 202) were extracted for a donor model, and bacteriopheophytin C-6 was extracted for an acceptor model. Hydrogen atoms were added with the program Titan (Wavefunction, Inc., Irvine, CA). In this procedure some sp^3 carbons were wrongly assigned as sp^2 carbons; these were edited by hand to sp^3 in the same program. The phytyl chains in both the bacteriochlorophyll and bacteriopheophytin molecules were replaced by methyl groups, and the histidine residues were edited to methylimidazol ligands. A spin-restricted computation with the TZP basis set and frozen first shells for carbon and oxygen was used for geometry optimization of the acceptor anion radical and a spin-restricted computation with the DZ basis set and frozen first shells for carbon and oxygen for the special pair donor cation radical. Hyperfine couplings were computed in spin-unrestricted computations with a TZ2P all-electron basis set for the acceptor anion radical and a TZP all-electron basis set for the donor cation radical. Spin-restricted spin−orbit relativistic computations within the ZORA formalism[52] were used for g tensor computations, employing a TZ2P all-electron basis set for the acceptor anion radical and a DZP basis set for the donor cation radical. Control computations of EPR parameters in the starting geometries revealed only slight changes in the parameters that are smaller than the expected accuracy of the DFT computations (±20% for hyperfine couplings, ±5° for principal axes directions). A full account of the DFT computations will be published elsewhere. For the donor cation radical, the computed g tensor principal axis directions could be compared to the experimental directions.[53] All three axes deviate by approximately 4° from the corresponding experimental axes, with the experimental errors being ±1−2°.

Chemical shift values for simulating photo-CIDNP spectra were taken from assignments made in this work (Table 2, values at 4.7 T) where possible. Missing values were taken from ref 24 if available there and from ref 54 otherwise (Table 1). Signals were represented by Gaussian peaks with a width of 0.5 ppm.

Results

Field Effects in the Dark Spectra. Figure 2 shows the spectra of the bacterial RC sample in the dark at three different

(45) Till, U.; Klenina, I. B.; Proskuryakov, I. I.; Hoff, A. J.; Hore, P. J. *J. Phys. Chem. B* **1997**, *101*, 10939−10948.
(46) Hulsebosch, R. J.; Borovykh, I. V.; Paschenko, S. V.; Gast, P.; Hoff, A. J. *J. Phys. Chem. B* **1999**, *103*, 6815−6823.
(47) Hulsebosch, R. J.; Borovykh, I. V.; Paschenko, S. V.; Gast, P.; Hoff, A. J. *J. Phys. Chem. B* **2001**, *105*, 10146−10146.
(48) Klette, R.; Torring, J. T.; Plato, M.; Mobius, K.; Bonigk, B.; Lubitz, W. *J. Phy. Chem.* **1993**, *97*, 2015−2020.
(49) Dorlet, P.; Rutherford, A. W.; Un, S. *Biochemistry* **2000**, *39*, 7826−7834.
(50) Velde, G. T.; Bickelhaupt, F. M.; Baerends, E. J.; Guerra, C. F.; Van Gisbergen, S. J. A.; Snijders, J. G.; Ziegler, T. *J. Comput. Chem.* **2001**, *22*, 931−967.
(51) Stowell, M. H. B.; McPhillips, T. M.; Rees, D. C.; Soltis, S. M.; Abresch, E.; Feher, G. *Science* **1997**, *276*, 812−816.
(52) van Lenthe, E.; Wormer, P. E. S.; van der Avoird, A. *J. Chem. Phys.* **1997**, *107*, 2488−2498.
(53) Huber, M. *Photosynth. Res.* **1997**, *52*, 1−26.
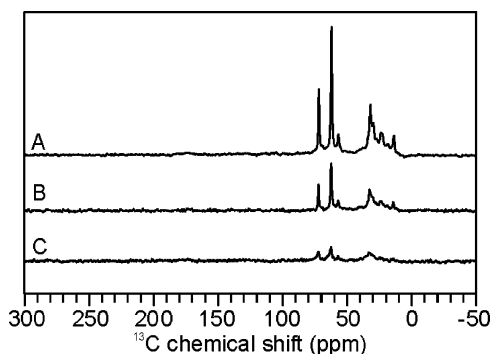(54) Facelli, J. C. *J. Phys. Chem. B* **1998**, *102*, 2111−2116.

Table 1. Chemical Shifts of BChl *a* and BPhe *a*

carbon no.	BChl *a*				BPhe *a*	
	$\sigma_{liq}{}^a$	$\sigma_{ss}{}^b$	$\sigma_{ss}{}^c$	$\sigma_{calcd}{}^d$	$\sigma_{ss}{}^c$	$\sigma_{calcd}{}^d$
3^1	199.3	194.5		203.4		190.2
13^1	189.0	188.2		197.1		188.1
17^3	173.4	174.0		187.2		191.9
13^3	171.6	171.4		183.7		162.8
6	168.9	170.2	166.8, 164.6	174.2	171.1	172.3
19	167.3	168.9	162.5, 159.7	174.4	169.9	168.4
14	160.8	160.7		164.7		147.4
9	158.5	158.0		162.8		167.2
16	152.2	150.1		160.1		162.6
1	151.2	153.5	148.2, 143.4	151.3	138.3	136.3
4	150.2	152.2		155.7		134.5
11	149.5	147.2	150.3, 154.2	160.6	138.9	140.3
2	142.1	140.7		150.8		132.1
3	137.7	136.1	130.2, 127.6	137.0	134.7	126.3
13	130.5	124.1	131.0, 131.3	134.4	126.4	125.6
12	123.9	119.9		132.9		120.4
15	109.7	105.8		119.0		110.6
10	102.4	100.0		109.5		99.6
5	99.6	98.8		106.4		101.7
20	96.3	93.7		105.9		97.2

^{a} The liquid NMR chemical shift data σ_{liq} have been obtained in acetone-d_6. ^{b} Matysik et al. (ref 23). ^{c} Schulten et al. (ref 24). ^{d} Facelli (ref 54).

magnetic fields: A, 17.6 T (750 MHz proton frequency); B, 9.4 T (400 MHz); and C, 4.7 T (200 MHz). All spectra have been recorded at a MAS rotational frequency of 8 kHz. The spectral quality obtained at 17.6 T is slightly above that obtained at 9.6 T. Both spectra A and B are clearly better resolved than spectrum C, obtained at 4.7 T. The observed field dependence of the signal-to-noise ratio and the spectral dispersion are in line with the expectations for NMR spectroscopy under Boltzmann conditions. Independent of those field effects, all dark spectra show similar features. All signals appear between 80 and 10 ppm. The amino acid backbone and aromatic carbons of aromatic amino acids and cofactors are hard to detect. The spectra are typical ^{13}C MAS NMR spectra of large proteins. No spinning sidebands are observed in the three spectra. This is due to the small CSA of aliphatic carbons and the small signal intensity of the carbonylic and aromatic signals.

Field Effects in the Light Spectra. Upon illumination, strong signals emerge in the aromatic region at all fields (Figure 3). All light-induced signals appear to be emissive (negative). Re-evaluation of previous photo-CIDNP data from WT[23,24] confirms this finding. This pattern is similar to that for photosystem I[25] and in contrast to those of RCs of *Rb. sphaeroides* R26[21,22,23] and of photosystem II[26,27] showing enhanced absorptive photo-CIDNP signals, except for the chemical shift range between 140 and 80 ppm where most signals appear emissive. The enhancement pattern in Figure 3 appears to be independent of the magnetic field strength, although the absolute enhancement factor is different at various fields. Spectrum A, obtained at 17.6 T, shows the weakest enhancement, whereas, in spectrum C, measured at 4.7 T, the strongest enhancement is observed. Using the signal from about 3300 methyl groups of the entire bacterial RC at 31 ppm as internal standard, enhancement factors of 60 (17.6 T), 1000 (9.4 T), and about 10000 (4.7 T) were computed.

Advantages of Measuring Photo-CIDNP at 4.7 T. The tremendously increased signal intensity at 4.7 T allows for data processing with less artificial line broadening (Figure 4). Therefore, spectrum C is better resolved than spectra A and B,

Figure 2. ^{13}C MAS NMR spectra of quinone depleted RCs of *Rb. sphaeroides* WT obtained at 223 K in the dark at different magnetic fields at 17.6 T (A), 9.4 T (B), and 4.7 T (C).
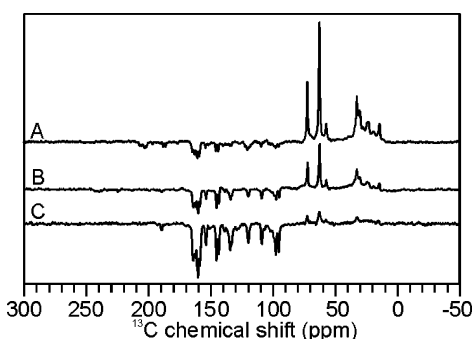

Figure 3. ^{13}C MAS NMR spectra of quinone depleted RCs of *Rb. sphaeroides* WT obtained at 223 K under illumination with continuous white light at different magnetic fields at 17.6 T (A), 9.4 T (B), and 4.7 T (C).
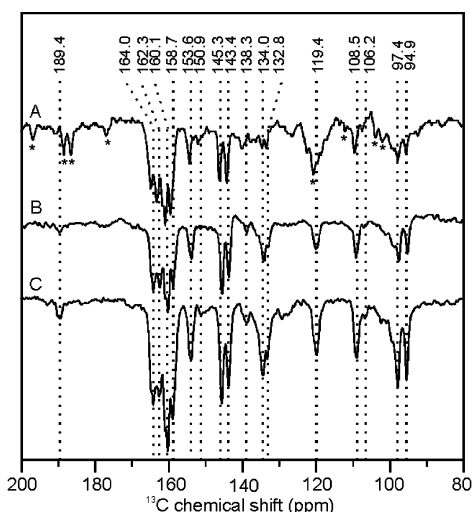

Figure 4. ^{13}C MAS NMR spectra of quinone depleted RCs of *Rb. sphaeroides* WT obtained at 223 K under illumination with continuous white light at different magnetic fields at 17.6 T (A), 9.4 T (B), and 4.7 T (C). Discussed centerbands are visualized by the dashed lines. Spinning sidebands are labeled by asterisks.

despite the decreased magnetic field strength which lowers signal dispersion on an absolute frequency scale. Note that spectral resolution obtained at 4.7 T is still limited by the necessity for some artificial line broadening imposed by the only moderate signal-to-noise ratio. Furthermore, the intensity of the spinning sidebands depends on the magnetic field strength. Those patterns can be easily observed in spectrum A (marked by asterisk), whereas no spinning sidebands are visible in
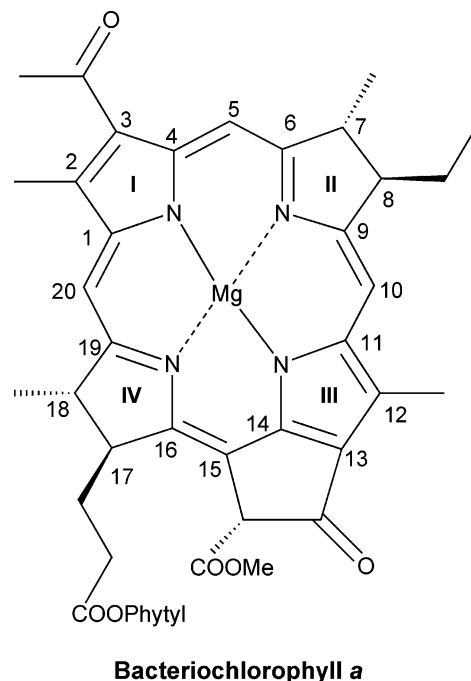

Bacteriochlorophyll *a*

Figure 5. Structure of a BChl *a* molecule with numbering of carbon atoms.

spectrum C. Finally, higher fields require longer general cycle delays. Therefore, photo-CIDNP MAS NMR experiments at the lower field provide (i) stronger signal intensity enhancement, (ii) lower signal widths, (iii) less spinning sidebands, and (iv) faster scanning.

Signal Assignments. At all three fields, the light-induced signals appear in the region of carbonyl and aromatic carbons, between 190 and 90 ppm. No light-induced signal is observed from aliphatic carbons. In Figure 4, the region of the light-induced signals is presented in detail. Some characteristic signals are marked by dashed lines. Table 1 compiles the ^{13}C chemical shift data of BChl *a* and BPhe *a* cofactors, on which our assignments are based. Figure 5 shows the numbering of the carbon atoms of a BChl *a* molecule.

The signal at 189.4 ppm, which can be observed in spectra B and C, can clearly be assigned to a carbonyl. Our simulations suggest an assignment to the carbonyl carbons C-Φ13[1] and C-Φ3[1] of the BPhe acceptor Φ. It is the first time that a carbonyl resonance has been detected in a bacterial RC. In spectrum A, the signal is hidden below spinning sidebands. Interestingly, in the photo-CIDNP spectrum of photosystem I showing a completely emissive set of light-induced signals, also an emissive signal of a C-13[1] carbonyl has been detected.[25]

In contrast to R26, a carbon C-6 of a BChl donor, appearing at about 170 ppm, cannot be detected in WT. The strongest signal appears at 160.1 ppm, as also observed in R26, belonging to the most prominent group, appearing between 165 and 155 ppm and being composed by at least five signals. These five signals can be conveniently assigned to the three carbons C-9, C-14, and C-19 of a donor BChl. The two additional signals can be arising from the second BChl of the special pair, demonstrating the difference in the electronic ground state of these two BChl cofactors.[24] Between 155 and 140 ppm, four signals can be clearly identified, which can be assigned tentatively to the carbons C-16 (150.9 ppm), C-1 (153.6 ppm),

C-11 (145.3 ppm), and C-2 (143.4 ppm). In contrast to R26, the signal at 148.5 ppm, assigned to a C-4,[23] cannot be observed in WT.

In the spectral range from 140 to 130 ppm, three signals can be resolved. For the weak signal at 138.3 ppm, which has not been observed in R26, the most straightforward assignment would be either a C-3 of a BChl donor or a C-Φ1 of a BPhe *a* acceptor. Our simulations suggest an assignment to the latter. The strong signal at 134.0 ppm has also been observed in R26 to be emissive and tentatively assigned to the C-ε of an axial histidine.[35] Alternatively, an assignment to a C-Φ2 of BPhe is possible. Also the weaker emissive signal at 132.8 ppm could either be assigned to a second axial histidine, to C-Φ2 of BPhe *a* or to a C-13 of BChl *a* or BPhe *a*. Similarly, the next significant signal appears at 119.4 ppm and may rise from a C-δ of an axial histidine or of a C-12 of BChl *a* or BPhe *a*. Comparison of all the safely assigned peaks in WT and R26 spectra suggests that signals of BChl *a* change from emissive to absorptive when going from WT to R26. The fact that both signals, at 134.0 and 119.4 ppm, appear emissive in R26 thus discourages an assignment to a BChl carbon. They would match very well to the shifts of C-δ and C-ε of a Mg-bound histidine[55,56] having similar distances to the BChl macrocycle. Histidines have indeed been observed by ^{15}N photo-CIDNP MAS NMR in R26; however, it was shown that the intensity has been obtained via spin-diffusion.[20] Furthermore, there is no hint from other spectroscopic methods for electron spin density on an axial histidine. Indeed, our simulations suggest an assignment of the signals at 134.0 and 119.4 ppm to the C-Φ2 and C-Φ12 carbons of BPhe *a*. A conclusive assignment to either axial histidines or the BPhe acceptor could be obtained from experiments with selective isotope labeling or with oriented samples.

Between 110 and 90 ppm, three strong emissive signals can be resolved at 108.5, 97.4, and 94.9 ppm. Furthermore, several weak features appear, for example, at 106.2 and 101.0 ppm, at which emissive signals have been observed in R26. Signals in this region can be assigned conveniently to methine carbons of BChl and BPhe cofactors. Assignment to histidines is unlikely since those resonances are not expected below 110 ppm. The enhancement pattern is rather different to that observed in R26, allowing identification of at least seven methine carbon resonances. Signals at 108.5 (prominent in WT) and 106.2 ppm (R26) can be assigned to C-15 carbons. The C-10 carbons may resonate at 101.0 (weakly observable in WT) and 101.0 ppm (R26). Signals at 99.2, 97.4, and 94.9 ppm can be assigned to C-5 and C-20 carbons. Simulations suggest that all three signals strongly appearing in WT arise from the BPhe acceptor. A full list of light-induced signals with their tentative assignments is given in Table 2.

Simulated CIDNP Spectra. To test for agreement between experiment and current theory of solid-state photo-CIDNP,[36] we have simulated spectra for the polarization arising from a single photocycle (Figure 6). As a substitute for the dark signal, peaks at 30 ppm with 250 times the thermal polarization of a single ^{13}C nucleus at the respective field were added (asterisks).

Table 2. Tentative Assignments of Observed Photo-CIDNP Signals[a]

cofactor and carbon no.	photo-CIDNP		
	$\sigma_{4.7T}$	$\sigma_{9.4T}$	$\sigma_{17.6T}$
Φ13[1]	189.4		
M6			
L19, M19	164.0	163.9	
?	162.3	162.3	
?	160.8	160.7	161.0
M14	160.1	160.1	159.3
L9, M9	158.7	158.6	158.0
L16, M16	150.9		
M1	153.6	153.6	153.0
M4			
M11	145.3	145.5	144.7
M2	143.4	143.6	142.9
Φ1, Φ3	138.3	138.7	
Φ2	134.0	133.9	
?	132.8	132.8	
Φ12	119.4	119.8	119.3
Φ15	108.5	109.1	108.4
Φ10, Φ5	101.8		
	97.4	97.3	96.5
Φ20	94.9	95.0	94.2

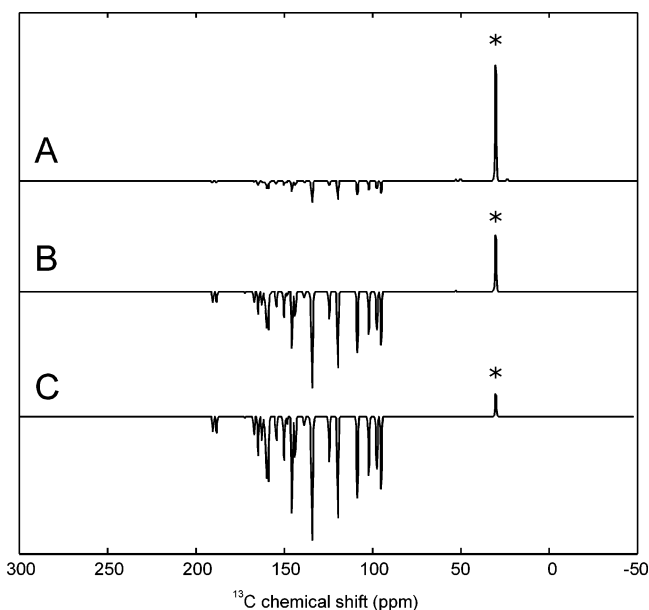[a] Φ = BPhe acceptor; L, M = BChl cofactors L and M of the special pair.

Figure 6. Simulated ^{13}C MAS NMR photo-CIDNP spectra corresponding to polarization generated in a single photocycle at 17.6 T (A), 9.4 T (B), and 4.7 T (C). The signals at 30 ppm (asterisks) were added for reference and correspond to 250 times the thermal polarization of a single ^{13}C nucleus at the respective field.

Field dependence of the photo-CIDNP amplitude is reproduced satisfactorily by these simulations (compare Figure 3). Also in agreement with the experiment, the intensity pattern depends only weakly on fields (see normalized detail plots in Figure 7). The number of significantly enhanced signals agrees quite well between experiment and simulation.

A more detailed comparison of the simulated and experimental patterns relies on the proper assignment of chemical shifts to the simulated peaks. The isotropic chemical shifts were originally taken from the reassigned solution data in ref 54. For carbons that were safely assigned by 2D NMR techniques in ref 24, these solution shifts were replaced by the solid-state isotropic shifts. For the remaining carbons the solution shifts

(55) Alia; Matysik, J.; Soede-Huijbregts, C.; Baldus, M.; Raap, J.; Lugtenburg, J.; Gast, P.; van Gorkom, H. J.; Hoff, A. J.; de Groot, H. J. M. *J. Am. Chem. Soc.* **2001**, *123*, 4803−4809.
(56) Alia; Matysik, J.; de Boer, I.; Gast, P.; van Gorkom, H. J.; de Groot, H. J. M. *J. Biomol. NMR* **2004**, *28*, 157−164.
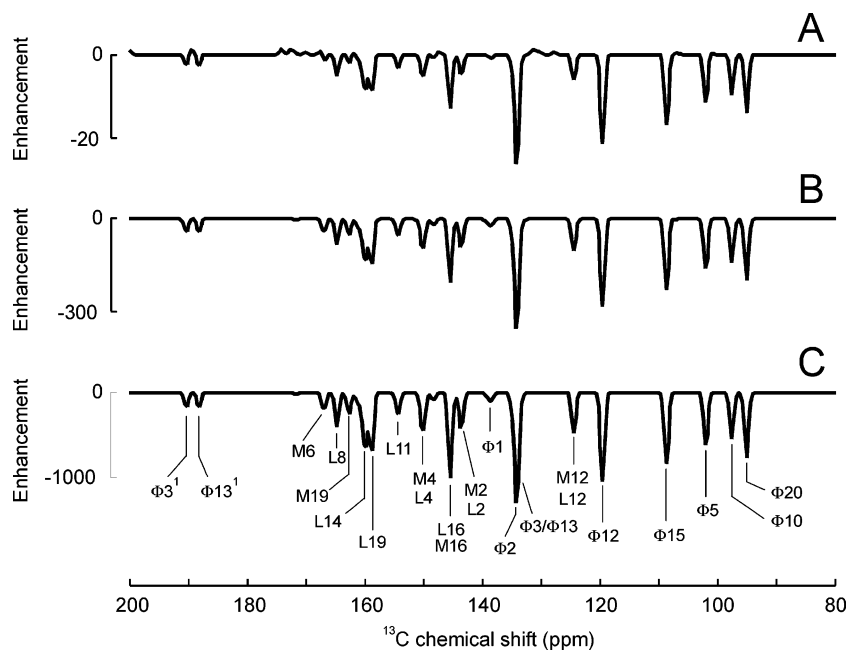
Figure 7. Details from the simulated ^{13}C MAS NMR photo-CIDNP spectra corresponding to polarization generated in a single photocycle at 17.6 T (A), 9.4 T (B), and 4.7 T (C). All spectra were normalized to the intensity of the largest peak at 132 ppm. Abbreviations: Φ = BPhe acceptor; L, M = BChl cofactors L and M of the special pair.

were corrected to solid-state shifts whenever a clear assignment had been made in the present work (see above). The assignment of all signals in the simulated spectrum is given in Figure 7C.

As the most obvious difference between experimental and simulated spectra, we note that the strongest enhancements in the simulated spectra are for carbon nuclei from the acceptor BPheo *a*, while in the experimental spectra, the strongest enhancements are observed for donor nuclei. Relative intensities of the acceptor Φ signals from carbons C-Φ1, C-Φ2, C-Φ3, C-Φ10, C-Φ12, C-Φ13, C-Φ15, and C-Φ20 in the simulation are in satisfying agreement with experiment, while the intensity of carbon C-Φ5 is clearly much smaller in the experiment than in the simulation. Interestingly, in the mutant strain R26 this signal does have the intensity expected from the simulation (see Figure 8). The relative intensity of the carbonyl signal at 189.1 ppm is in quite good agreement with the intensities simulated for the acceptor carbonyls C-Φ3[1] and C-Φ13[1], although it has to be said that in the simulations two carbonyl signals are seen at all fields, while in the experimental spectra only one such signal is observed at 4.7 and 9.4 T.

For the signals assigned to the donor, agreement of relative intensities between experiment and simulation is clearly worse than that for the acceptor signals. In particular, the signal of carbons C-M12 and C-L12 at 124.3 ppm is not observed experimentally at any field, except possibly at 17.6 T. Similarly, the signal of C-M4 and C-L4 at 149.9 ppm is hardly significant in the experimental spectra. In contrast, the group of signals between 153 and 165 ppm has lower intensity in the simulation than in the experiment. However, most of the expected signals are indeed observed with relative intensities that do not differ too strongly from the simulations. All experimentally observed signals can be assigned to carbon nuclei that do exhibit strong signal enhancements in the simulations.

Comparison to R26. In WT all signals are emissive, whereas in R26 all low-frequency signals are absorptive and the signals at 132.8, 119.4 as well as all methine carbon resonances are
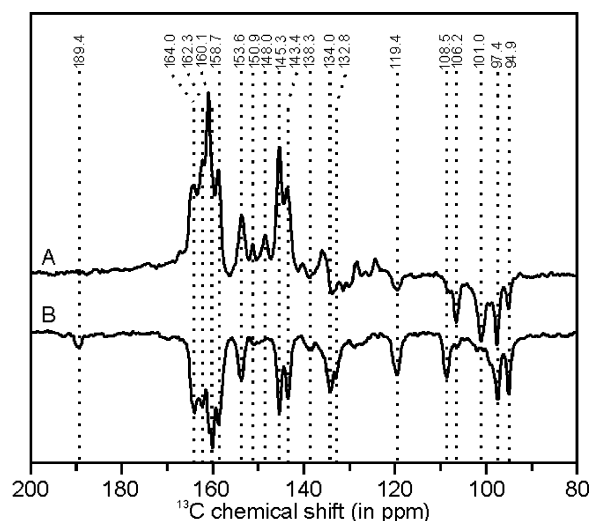

Figure 8. Comparison of ^{13}C MAS NMR photo-CIDNP spectra of bacterial photosynthetic reaction centers: (A) Carotinoidless mutant strain R26. (B) Wild type.

emissive (Figure 8). In both WT and R26, the strongest photo-CIDNP signal appears at 160.8 ppm, however with opposite sign. The overall envelopes in the low-frequency region of the emissive photo-CIDNP spectrum of WT and the enhanced absorptive photo-CIDNP spectrum of R26 appear to be similar. Our tentative assignments (Table 2, Figure 6C) suggest that, compared to the WT spectrum, donor signals in R26 have opposite sign while acceptor signals are hardly changed. Interestingly, at shifts where the signals of carbons C-Φ5 (101.0 ppm), C-M12/L12 (124 ppm), and C-M4/L4 (150.9 ppm) are expected from the simulations but not observed in WT, peaks appear in R26.

Experimental photo-CIDNP enhancements are by a factor of 10 higher than enhancements simulated for a single photocycle. This implies that the rate of photon absorption by a given RC

is by at least a factor of 10 faster than the rate of longitudinal nuclear relaxation. As true photon absorption rates are difficult to estimate, we refrain here from a quantitative discussion of the absolute enhancement factors.

Discussion

Electronic Structure of the Radical Pair. The photo-CIDNP data presented here are obtained from unlabeled RCs. Therefore, the obtained photo-CIDNP intensities cannot be equalized by spin-diffusion processes but refer to the electron spin densities localized at the particular carbon atoms. Until now, signal assignments were difficult to check due to a lack of simulation methods. Here we obtain broad agreement of the number of signals, many relative intensities, and most expected chemical shifts between experiment and simulation. Hence, we can demonstrate for the first time that photo-CIDNP MAS NMR allows us to study the radical pair state of a RC at atomic resolution, whereas other methods are usually limited to molecular resolution.

Based on ^{1}H ENDOR data, an electron spin density distribution of the two donor BChl cofactors of 2:1 in favor of cofactor L in the active branch has been modeled for R26.[57] Our DFT computations suggest an electron spin density distribution of 3:2 in favor of cofactor L. Theoretical considerations show that, for a polarization transfer based on the pseudosecular hyperfine coupling, the leading term of nuclear polarization is proportional to the square of the anisotropy of the hyperfine coupling.[37] One may thus expect that signals from cofactor L are by a factor of $1.5^2 = 2.25$ stronger than those of cofactor M. In good agreement with this expectation we find intensity ratios in the range 2 to 2.5 for equivalent carbon atoms in the L and M cofactor in the simulations. Experimental resolution does not yet permit the extraction of reliable relative intensities of signals from equivalent carbons in the L and M cofactor from the experimental spectra. An experimental determination of this ratio should be feasible using a ^{13}C-labeled sample with the labeling pattern of ref 24, as signals C-M19 and C-L19 should then be resolved.

Interestingly the electron density distribution is significantly asymmetric in our DFT computation that neglects all matrix effects except for histidine coordination. Closer examination of the structures shows that the two cofactors differ in deviations of the macrocycle from planarity and in sidegroup conformations. These differences are very likely imposed by the matrix. They appear to correspond to sufficiently deep local minima on the energy hypersurface to be stable in a geometry optimization by DFT. The sidegroups in chlorophylls and pheophytins might thus be levers used by nature for fine-tuning of the electronic structure of these pigments or their assemblies.

It is somewhat surprising that enhanced aromatic signals of the BPhe *a* macrocycle are almost exclusively situated at lower shifts than those of the BChl *a* macrocycles. Possibly this is related to a correlation between electronic ground state and radical electron densities. The strongly enhanced nuclei in BPhe *a* correspond to high spin density in an anion radical, whose singly occupied molecular orbital (SOMO) is related to the lowest unoccupied molecular orbital (LUMO) of the ground
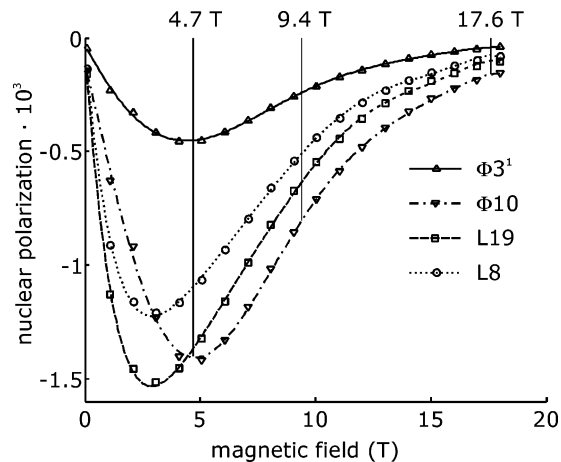

Figure 9. Simulated field dependence of ^{13}C NMR photo-CIDNP effects for nuclei C-$\Phi 3^1$ and C-$\Phi 10$ of the BPheo *a* (acceptor) and C-L8 and C-L19 of BChl *a* (cofactor L of the special pair donor). Computed values are plotted as marker symbols; lines are guides to the eyes.

state. Conversely, enhanced signals in BChl *a* correspond to high spin density in a cation radical, whose SOMO is related to the highest occupied molecular orbital (HOMO) of the ground state.

Strongest Effect. For carbons C-$\Phi 3^1$, C-$\Phi 10$, C-L8, and C-L19, we have computed the photo-CIDNP effect as a function of the magnetic field B_0 in steps of 1 T (Figure 9). The maximum absolute nuclear polarization is obtained at fields between 3 and 5 T. Field dependence of detection sensitivity for constant polarization follows a scaling law with an exponent between 1 and 7/4.[58] Even with $B_0^{7/4}$ scaling, the maxima of photo-CIDNP sensitivity virtually coincide with the maxima of absolute nuclear polarization. Therefore, photo-CIDNP ^{13}C MAS NMR experiments at fields between 3 and 5 T are expected to provide the best sensitivity. The photo-CIDNP enhancement with respect to thermal polarization increases monotonically with decreasing field (data not shown). Photo-CIDNP signals that overlap with dark signals may thus be easier to recognize at even lower fields.

We have also checked by simulations for selected nuclei how much of the polarization is contributed by the individual mechanisms. For instance, the total polarization of −1238 times thermal equilibrium polarization (TEP) for carbon C-$\Phi 2$ is composed of a larger negative contribution from the TSM mechanism (−1449 TEP) and a smaller positive contribution from the DD mechanism (211 TEP). For carbon C-L16, the total polarization of −727 TEP is made up of a TSM contribution of −603 TEP and a DD contribution of −124 TEP. For donor nuclei, the DD and TSM contributions have the same sign, while they counteract each other for acceptor nuclei. This is because the sign of the DD contribution depends on the sign of the *g* value difference,[36] which is opposite for acceptor and donor nuclei.

Completeness of Theory. Several relevant parameters, such as exchange and dipole−dipole coupling between the two electron spins and lifetimes of singlet and triplet pairs, are known with only limited precision. Furthermore, principal axes directions of interaction tensors computed by DFT may deviate from true directions by a few degrees, and hyperfine couplings

(57) Lendzian, F.; Huber, M.; Isaacson, R. A.; Endeward, B.; Plato, M.; Bonigk, B.; Möbius, K.; Lubitz, W.; Feher, G. *Biochim. Biophys. Acta* **1993**, *1183*, 139−160.

(58) Minard, K. R.; Wind, R. A. *Concepts Magn. Reson.* **2001**, *13*, 190−210.

computed by DFT may well deviate by 20−30% from true values for the computed molecule and geometry. The neglect of the protein matrix, except for the directly coordinated histidines, may introduce further errors of the hyperfine couplings, and possibly even into the detailed spin density distribution over the molecule. Considering all these uncertainties, the agreement of the simulated and experimental photo-CIDNP spectra for WT reaction centers is as good as it can be expected.

The same is not true for spectra of R26 reaction centers. Even when varying *J* coupling, dipole−dipole coupling, and radical pair lifetimes within reasonable ranges, we cannot reproduce the pattern of mainly absorptive donor polarization and mainly emissive acceptor polarization that we observe experimentally. In fact, we do not find any parameter set that produces both strong emissive and strong absorptive polarization for any assignment of nuclei. This finding and the fact that even in WT the agreement is worse for donor than for acceptor nuclei suggest that nuclear polarization changes during the lifetime of the donor triplet. In WT, where this lifetime is only 100 ns, the changes are relatively minor. Apparently, the emissive polarization of donor nuclei is somewhat enhanced, as it is larger than expected relative to acceptor polarization. In R26, where the triplet lifetime is 100 μs, donor polarization changes sign, although relative intensities change only slightly.

A detailed study of possible mechanisms for polarization buildup during the triplet lifetime is beyond the scope of this paper. We may remark that, in contrast to the situation in the radical pair, in the triplet state transfer of electron spin polarization to nuclear polarization by coherent spin evolution is negligible. This is because in the triplet state there is no near degeneracy of levels with different electron spin quantum numbers that could be mixed by the hyperfine interaction. Hence it is more likely that the additional polarization is generated from chemically induced nuclear coherence (CIDNC).[59] In the radical pair state, buildup of CIDNC is expected to be stronger than buildup of CIDNP.[36] As the hyperfine field at the nuclei is negligible in the T_0 manifold of the donor triplet but has significant pseudo-secular components in the T_{-1} and T_{+1} manifolds, CIDNC is transferred to CIDNP to a significant extent if and only if recombination of the triplet radical pair also populates T_{-1} or T_{+1} sublevels. This consideration is supported by preliminary simulations. Depending on the relative populations of T_{-1} or T_{+1} sublevels, such a mechanism could explain the sign change. It could also explain that relative intensities change only slightly. Further theoretical and experimental work is needed to prove or refute this mechanism.

JA054015E

(59) Jeschke, G. *J. Chem. Phys.* **1997**, *106*, 10072−10086.